J. Fluid Mech. (1986), *vol.* 167, *pp.* 95–115
Printed in Great Britain

A moment model for vortex interactions of the two-dimensional Euler equations. Part 1. Computational validation of a Hamiltonian elliptical representation

By M. V. MELANDER, N. J. ZABUSKY AND A. S. STYCZEK†
Institute for Computational Mathematics and Applications, Department of Mathematics and Statistics, University of Pittsburgh, Pittsburgh, Pennsylvania 15260

(Received 22 April 1985 and in revised form 19 September 1985)

We consider the evolution of finite uniform-vorticity regions in an unbounded inviscid fluid. We perform a perturbation analysis based on the assumption that the regions are remote from each other and nearly circular. Thereby we obtain a self-consistent infinite system of ordinary differential equations governing the physical-space moments of the individual regions. Truncation yields an Nth-order moment model. Special attention is given to the second-order model where each region is assumed elliptical. The equations of motion conserve local area, global centroid, total angular impulse and global excess energy, and the system can be written in canonical Hamiltonian form. Computational comparison with solutions to the contour-dynamical representation of the Euler equations shows that the model is useful and accurate. Because of the internal degrees of freedom, namely aspect ratio and orientation, two like-signed vorticity regions collapse if they are near each other. Although the model becomes invalid during a collapse, we find a striking similarity with the merger process of the Euler equations.

1. Introduction

Ideally, one wishes to solve the 2-dimensional Euler equations for realistic initial conditions in bounded and unbounded domains. However, there is no algorithm for all seasons. In recent years the continuum equations have been represented by finite-difference, finite-element, pseudospectral and particle-in-cell algorithms. At the other extreme, mathematical and physical insight has been obtained from 'point' vortex and invariant-core vortex (ICV) models (also called 'blob' models). Recently, Zabusky and colleagues introduced the contour-dynamics (CD) approach as an intermediate representation for the Euler equations. Here, piecewise-constant *finite-area vortex regions* which we call FAVORs can be described rigorously by the motion of the contour bounding the regions. One expects that the limit of a many-nested contour region would give solutions that approach continuum solutions of the Euler equations. In any case, one-contour representations have provided a richness of mathematical and physical insights, mainly through computation. For a recent discussion of some of these developments see the reviews by Leonard (1980), Aref (1983) and Zabusky (1984).

The equations for a point-vortex representation define a Hamiltonian system. They have been used for linear and nonlinear stability studies and in recent years for

† Permanent address: Institut Techniki Cieplnej, Politechnika Warszawska, Warsaw, Poland.

investigations of chaotic behaviour. However, because of their singular nature, they are computationally undesirable, and circular ICVs have been used, as reviewed by Leonard (1980). Recently, nice results on convergence to the continuum have been obtained if the core radius $\delta \propto h^q$, where h is the mean intercore distance and $q < 1$. That is, the particles overlap strongly in the limit of decreasing h. However, few *cogent* computations exist – namely, those that are computationally demanding, of sufficient duration and carefully diagnosed. For example, Beale & Majda (1984) have examined the evolution of smooth *circular* symmetric states for up to 4.5 eddy turnaround times with 208 particles. A more demanding calculation by Nakamura, Leonard & Spalart (1982) investigated the evolution of a 4/3 elliptical FAVOR that was approximated with 256 vortices. However, only one period of rotation was examined.

In §2 we propose a model of well-separated vortex entities – each assumed to be an almost circular FAVOR. Under these assumptions a perturbation analysis leads to an infinite system of coupled ordinary differential equations for physical-space moments of the individual regions. If truncated, a self-consistent closed model is obtained at any order. Unlike the ICV model, the accuracy is not obtained by overlap of cores but through the excitation of internal degrees of freedom on each FAVOR.

In §3 we discuss the simplest second-order model obtained by omitting third- and higher-order moments. For the following mathematical and physical reasons, we represent the second-order moments of each region by an *elliptical* FAVOR. The isolated elliptical FAVOR – Kirchoff's elliptical vortex – is a steady state solution of the Euler equations. Kida (1981) found that the isolated elliptical shape is preserved exactly in an arbitrary strain field, $\boldsymbol{u}_s = A\boldsymbol{x}\boldsymbol{e}_x - B\boldsymbol{y}\boldsymbol{e}_y$, even as the aspect ratio and orientation vary in time. Neu (1984) generalized these considerations of elliptical vortices by including an out-of-plane strain velocity component. McWilliams (1984), in 2-dimensional pseudospectral simulations, found that localized elliptically shaped regions of vorticity of various sizes emerge from initial conditions with power-law spectra and random phases. When these vortical regions become well-separated they approach circular symmetry. Furthermore, from CD (Overman & Zabusky 1982) and high-resolution pseudospectral (Melander, McWilliams & Zabusky 1986) simulations, we find a near-elliptical shape emerge from two closely interacting, initially circular vorticity distributions. Also, image-processing methods have been used by Hernan & Jimenez (1982) to study data from free-shear-layer experiments, and the elliptical shape has been found to be a reasonable and computationally convenient form. Thus we have a low-order model where each FAVOR is characterized by its centroid position, aspect ratio and orientation. The two internal degrees of freedom are sufficient to capture aspects of the often observed convective merger (Winant & Browand 1974). Using the second-order model, we observe that two like-signed FAVORs approach and 'collapse' (their intercentroid distance vanishes) within a finite time, provided they are initially sufficiently close together. We find agreement between critical 'collapse' distances of the model and critical merger distances of the Euler equations.

In §4 we examine the conservation laws of the model. We find that the local area, local centroid and the total angular impulse are conserved for any order of the model. For the second-order model the energy is also conserved. In fact this model forms a Hamiltonian system.

Section 5 compares the model's doubly connected corotating and translating steady-state solutions against those of the Euler equations. Finally, we examine evolutions and validate them by comparing against CD-results.

A brief and preliminary account of this work was published by Melander, Styczek & Zabusky (1984).

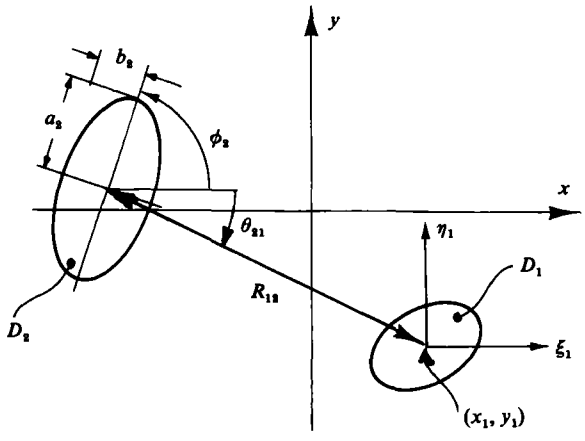

FIGURE 1. The parameters defining the geometry for interacting FAVORs. Shown are two elliptical regions D_1 and D_2 with aspect ratios $\lambda_1 = a_1/b_1$ and $\lambda_2 = a_2/b_2$ introduced in the second-order moment model in §3.

2. Formulation of a moment model

We consider N domains D_k (FAVORs) of area A_k and vorticity ω_k on the (x, y)-plane. For convenience, we choose the origin as the centroid of global vorticity (except of course when the centroid is at infinity). We introduce N *local* coordinate systems (ξ_k, η_k), one for each domain D_k. The origin of the kth coordinate system is at $\boldsymbol{x}_k$, the centroid of the kth FAVOR and the axes are parallel to the inertial system axes as shown in figure 1.

Our goal is to formulate evolution equations for the centroid $\boldsymbol{x}_k$ and the local geometrical moments

$$J_k^{(m,n)} \equiv \int_{D_k} \xi_k^m \eta_k^n \, \mathrm{d}\sigma. \tag{2.1}$$

In order to obtain these equations we apply perturbation techniques that require the following.

H1: The maximum diameter of any FAVOR is much smaller than the minimum distance between any two centroids.

H2: The centroid of any FAVOR is within the FAVOR itself.

These conditions must be satisfied by the initial conditions. As time evolves, one or both conditions may be violated and our approach will become invalid. The first condition requires that the FAVORs be well-separated and allows us to introduce the perturbation parameter

$$\epsilon \equiv \text{maximum FAVOR diameter/minimum intercentroid distance}, \tag{2.2}$$

which is time dependent. At $t = 0$ we choose the minimum intercentroid distance as a characteristic unit length. Thereby ϵ becomes a small parameter if H1 is valid. Thus

$$J_k^{(m,n)} = O(\epsilon^{m+n+2}), \tag{2.3}$$

and we have a basis for omitting higher-order moments in our perturbation procedure.

Assumption H2 enables us to introduce another perturbation parameter, d_k, which

is used in the self-interaction computation. Let y be a point on the boundary of the kth FAVOR; then we define a mean radius of the FAVOR by

$$r_k \equiv \tfrac{1}{2}(\max|y-x_k| + \min|y-x_k|) \tag{2.4}$$

and

$$d_k = \frac{|y-x_k|^2}{pr_k^2} - 1. \tag{2.5}$$

Here $p > 1$ is a constant that we introduce because of convergence considerations. d_k is used in the power-series expansion $\ln(1+d_k) = d_k - \frac{1}{2}d_k^2 + \ldots$. If $p \geqslant 2$ then $|d_k| < 1$, because of H2, and the series is convergent, but is not an asymptotic expansion about $|y-x_k| = r_k$. If $p = 1$ the series becomes an asymptotic expansion. However, $|d_k|$ might be larger than unity, causing the series to be divergent.

The incompressible Euler equations, in vorticity/stream function form are

$$\frac{D\omega}{Dt} \equiv \omega_t + u\omega_x + v\omega_y = 0, \quad \Delta\psi = -\omega, \tag{2.6}$$

where the velocity field is

$$u \equiv (u, v) = (\psi_y, -\psi_x).$$

In order to apply perturbation techniques, we decompose the velocity field u into a near field u_k and a far field U_k:

$$u = u_k + U_k, \tag{2.7}$$

where the near field is generated only by the kth FAVOR, whereas the far field is due to the remaining remote FAVORs. Both velocity fields can be expressed in terms of stream functions:

$$u_k = (\partial_y \psi_k, -\partial_x \psi_k),$$

$$U_k = (\partial_y \Psi_k, -\partial_x \Psi_k).$$

where

$$\psi_k(x) = -\frac{\omega_k}{2\pi}\int_{D_k} \ln|x_k + \xi_k - x|\,d\sigma \tag{2.8}$$

and

$$\Psi_k(x) = -\sum_{\alpha=1}^{N}{}' \frac{\omega_\alpha}{2\pi}\int_{D_\alpha} \ln|x_\alpha + \xi_\alpha - x|\,d\sigma. \tag{2.9}$$

The prime means $\alpha \neq k$.

The area A_k of each domain is an invariant because $(D/Dt)\int_{D_k}\omega\,d\sigma = 0$ (Kelvin's theorem). The centroid of the kth FAVOR is defined by

$$A_k x_k = \int_{D_k} x\,d\sigma, \tag{2.10}$$

and we obtain the evolution equation for x_k by differentiating with respect to time:

$$A_k \dot{x}_k = \frac{d}{dt}\int_{D_k} x\,d\sigma = \int_{D_k}\frac{D}{Dt}x\,d\sigma = \int_{D_k} u\,d\sigma$$

$$= \int_{D_k}(u_k + U_k)\,d\sigma = \int_{D_k} U_k\,d\sigma.$$

Here we have used the fact that a FAVOR cannot displace its own centroid, i.e. the centroid motion is governed by the far field only. If we expand $U_k(x)$ about x_k we obtain

$$\dot{x}_k = A_k^{-1}\sum_{q=0}^{\infty}\sum_{p=0}^{q}\frac{1}{p!(q-p)!}J_k^{(p,q-p)}\,\partial_x^p\,\partial_y^{q-p}\,U_k\Big|_{x_k}. \tag{2.11}$$

We derive the evolution equation for the local geometrical moments in a similar manner. Starting from the definition (2.1), we have

$$\begin{aligned}
\dot{J}_k^{(m,n)} &= \frac{\mathrm{d}}{\mathrm{d}t}\int_{D_k}\xi_k^m\,\eta_k^n\,\mathrm{d}\sigma = \int_{D_k}\frac{\mathrm{D}}{\mathrm{D}t}(\xi_k^m\,\eta_k^n)\,\mathrm{d}\sigma \\
&= \int_{D_k}\left[m\eta_k^n\,\xi_k^{m-1}\frac{\mathrm{D}\xi_k}{\mathrm{D}t}+n\eta_k^{n-1}\,\xi_k^m\,\frac{\mathrm{D}\eta_k}{\mathrm{D}t}\right]\mathrm{d}\sigma \\
&= \int_{D_k}\eta_k^{n-1}\xi_k^{m-1}\left[m\eta_k\,\frac{\mathrm{D}}{\mathrm{D}t}(x-x_k)+n\xi_k\frac{\mathrm{D}}{\mathrm{D}t}(y-y_k)\right]\mathrm{d}\sigma \\
&= \int_{D_k}\eta_k^{n-1}\,\xi_k^{m-1}\,[m\eta_k(u-\dot{x}_k)+n\xi_k(v-\dot{y}_k)]\,\mathrm{d}\sigma \\
&= \dot{J}_{*k}^{(m,n)}+\int_{D_k}\eta_k^{n-1}\,\xi_k^{m-1}\,[m\eta_\kappa(U_k-\dot{x}_k)+n\xi_\kappa(V_k-\dot{y}_k)]\,\mathrm{d}\sigma, \qquad (2.12)
\end{aligned}$$

where

$$\dot{J}_{*k}^{(m,n)} \equiv \int_{D_k}(\eta_k^{n-1}\,\xi_k^{m-1})\,(m\eta_k\,u_k+n\xi_k\,v_k)\,\mathrm{d}\sigma, \qquad (2.13)$$

represents the kth FAVORs self-interaction, while the second term describes the influence of the other FAVORs. Now we expand $\boldsymbol{U}_k$ and $\boldsymbol{u}_k$ around $\boldsymbol{x}_k$, so that we can express the integrals in (2.12) in terms of the local geometrical moments.

For convenience, we write the far-field stream function Ψ_k as a sum of normalized stream functions $\Psi_{k\alpha}$, one for each of the remote FAVORs, or

$$\Psi_k(\boldsymbol{x}) = -\sum_{\alpha=1}^{N}{}'\,\frac{\omega_\alpha}{2\pi}\,\Psi_{k\alpha}(\boldsymbol{x}), \qquad (2.14)$$

where

$$\Psi_{k\alpha}(\boldsymbol{x}) = \int_{D_\alpha}\ln|\boldsymbol{x}_\alpha+\boldsymbol{\xi}_\alpha-\boldsymbol{x}|\,\mathrm{d}\sigma. \qquad (2.15)$$

Because of (H1), all FAVORs are well-separated, or $|\boldsymbol{x}_\alpha-\boldsymbol{x}| \gg |\boldsymbol{\xi}_\alpha|$ for $\boldsymbol{x}\in D_k$. Hence we expand the logarithm in (2.15):

$$\begin{aligned}
\Psi_{k\alpha}(\boldsymbol{x}) &= \ln|\boldsymbol{x}-\boldsymbol{x}_\alpha|\int_{D_\alpha}\mathrm{d}\sigma-\sum_{n=1}^{\infty}\frac{1}{2n}\int_{D_\alpha}\left[\frac{2(x-x_\alpha)\,\xi_\alpha+2(y-y_\alpha)\,\eta_\alpha-\xi_\alpha^2-\eta_\alpha^2}{|\boldsymbol{x}-\boldsymbol{x}_\alpha|^2}\right]^n\mathrm{d}\sigma \\
&= J_\alpha^{(0,0)}\ln|\boldsymbol{x}-\boldsymbol{x}_\alpha| \\
&\quad+\frac{((y-y_\alpha)^2-(x-x_\alpha)^2)\,J_\alpha^{(2,0)}-4(x-x_\alpha)\,(y-y_\alpha)\,J_\alpha^{(1,1)}+((x-x_\alpha)^2-(y-y_\alpha)^2)\,J_\alpha^{(0,2)}}{2\,|\boldsymbol{x}-\boldsymbol{x}_\alpha|^4} \\
&\quad+\ldots. \qquad (2.16)
\end{aligned}$$

Thus the far-field velocity is obtained from Ψ_k by substituting (2.16) into (2.14).

Similarly, the near-field velocity is used to obtain the evolution of $J_{*k}^{(m,n)}$ in (2.13), namely

$$\begin{aligned}
\dot{J}_{*k}^{(m,n)} &= m(J_k^{(m,n)}\,u_\xi|_{x_k}+J_k^{(m-1,n+1)}u_\eta|_{x_k}) \\
&\quad+n(J_k^{(m+1,n-1)}v_\xi|_{x_k}+J_k^{(m,n)}v_\eta|_{x_k})+\ldots, \qquad (2.17)
\end{aligned}$$

where $\boldsymbol{u}_k(\boldsymbol{x})$ has been expanded about $\boldsymbol{x}_k$ or

$$\boldsymbol{u}_k = [\xi_k\,\partial_\xi\boldsymbol{u}_k+\eta_k\,\partial_\eta\boldsymbol{u}_k+\ldots]|_{\xi=0}. \qquad (2.18)$$

This expansion contains the mixed derivatives

$$\partial_\xi^p \partial_\eta^q \boldsymbol{u}_k|_{x_k} = -\frac{\omega_k}{4\pi}\Big[\int_{D_k} \partial_\xi^p \partial_\eta^q (\partial_\eta, -\partial_\xi) \ln|\xi_k - \xi|^2 \,\mathrm{d}\sigma\Big]\Big|_{\xi=0}.$$

To show that the singularity is only apparent, we use Green's theorem and convert to a line integral

$$\begin{aligned}\partial_\xi^p \partial_\eta^q \boldsymbol{u}_k|_{x_k} &= +\frac{\omega_k}{4\pi}\Big[\int_{\partial D_k} \partial_\xi^p \partial_\eta^q \ln|\xi - \xi_k|^2 \,\mathrm{d}\xi_k\Big]\Big|_{\xi=0} \\ &= +\frac{\omega_k}{4\pi}\int_{\partial D_k} \partial_\xi^p \partial_\eta^q \ln(\xi_k^2+\eta_k^2)\,\mathrm{d}\xi_k. \end{aligned} \tag{2.19}$$

Because of H2, the centroid of the kth FAVOR is not on the boundary (i.e. $\xi_k^2+\eta_k^2 > 0$), and we expand the logarithm as discussed above:

$$\ln(\xi^2+\eta^2) \equiv \ln r^2 = \ln r_k^2 + \Big[\Big(\frac{r}{r_k}\Big)^2 - 1\Big] - \frac{1}{2}\Big[\Big(\frac{r}{r_k}\Big)^2 - 1\Big]^2 + \ldots, \tag{2.20}$$

where r_k is a mean radius defined in (2.4). We substitute into (2.19) and convert back to a domain integral which provides us with a moment expansion

$$\partial_\xi^p \partial_\eta^q \boldsymbol{u}_k|_{x_k} = -\frac{\omega_k}{4\pi}\int_{D_k} (\partial_\eta, -\partial_\xi)\,\partial_\xi^p \partial_\eta^q \Big\{\Big[\Big(\frac{r}{r_k}\Big)^2 - 1\Big] - \frac{1}{2}\Big[\Big(\frac{r}{r_k}\Big)^2 - 1\Big]^2 + \ldots\Big\}\,\mathrm{d}\sigma. \tag{2.21}$$

In lowest order this is

$$\partial_\xi \boldsymbol{u}_k|_{x_k} = \frac{\omega_k}{\pi}\Big(\frac{J_k^{(1,1)}}{r_k^4}, +\frac{A_k}{r_k^2} - \frac{J_k^{(0,2)} + 3J_k^{(2,0)}}{2r_k^4}\Big), \tag{2.22a}$$

$$\partial_\eta \boldsymbol{u}_k|_{x_k} = -\frac{\omega_k}{\pi}\Big(\frac{A_k}{r_k^2} - \frac{J_k^{(2,0)} + 3J_k^{(0,2)}}{2r_k^4}, \frac{J_k^{(1,1)}}{r_k^4}\Big), \tag{2.22b}$$

which when substituted into (2.17) yields our lowest self-interaction terms. We can combine results and write (2.12) as

$$\begin{aligned}\dot{J}_k^{(m,n)} = J_{*k}^{(m,n)} &+ \{[-(nJ^{(m+1,n-1)})\,\partial_x^2 + (m-n)\,J_k^{(m,n)}\,\partial_x\partial_y \\ &+ (mJ_k^{(m-1,n+1)})\,\partial_y^2] + \ldots + \tfrac{1}{2}A_k^{-1}[-mJ_k^{(m-1,n)}\,\partial_y + nJ_k^{(m,n-1)}\,\partial_x] \\ &\times [J_k^{(2,0)}\,\partial_x^2 + 2J_k^{(1,1)}\,\partial_x\partial_y + J_k^{(0,2)}\,\partial_y^2 + \ldots]\}\,\Psi_k|_{x_k}. \end{aligned} \tag{2.23}$$

Equations (2.23) and (2.11) constitute an infinite system of ordinary differential equations. Since we do not know the shape of the FAVORs, we are not able to calculate r_k. Thus we use the approximation $\tilde{r}_k = (A_k/\pi)^{\frac{1}{2}}$. This, however, has the disadvantage that we cannot be sure of the convergence of (2.20) for FAVORs that are extremely distorted from circular symmetry.

3. The second-order moment model

We make the system of equations (2.11) and (2.23) finite and closed in any order by omitting all terms of higher order. If we omit second- and higher-order moments we obtain the well-known point-vortex model. The second-order model has three interrelated moments which define an ellipse. As discussed in §1, nearly elliptical vortex regions arise frequently in laboratory experiments and computer simulations.

Furthermore, the isolated elliptical FAVOR (Kirchhoff's elliptical vortex) is a steady-state solution rotating with constant angular velocity

$$\Omega = \omega\lambda/(1+\lambda)^2, \tag{3.1}$$

where λ is the aspect ratio of the ellipse. Thus the second-order model is exceptional because we can use (3.1) for self-interaction velocity calculations instead of the expansion of (2.17).

The moments of inertia for an ellipse with aspect ratio $\lambda = a/b$ and with the major axis tilted at ϕ are

$$J^{(2,0)} = \frac{A^2}{4\pi\lambda}(\lambda^2 + (1-\lambda^2)\sin^2\phi), \tag{3.2}$$

$$J^{(0,2)} = \frac{A^2}{4\pi\lambda}(\lambda^2 + (1-\lambda^2)\cos^2\phi), \tag{3.3}$$

$$J^{(1,1)} = -\frac{A^2}{8\pi\lambda}(1-\lambda^2)\sin 2\phi. \tag{3.4}$$

Using (3.1), we find that the self-interaction can be expressed as

$$\mathring{J}^{(2,0)}_{*} = \frac{\omega A^2}{4\pi}\frac{1-\lambda}{1+\lambda}\sin 2\phi, \tag{3.5}$$

$$\mathring{J}^{(0,2)}_{*} = -\mathring{J}^{(2,0)}_{*}, \tag{3.6}$$

$$\mathring{J}^{(1,1)}_{*} = -\frac{\omega A^2}{4\pi}\frac{1-\lambda}{1+\lambda}\cos 2\phi. \tag{3.7}$$

From §2 we obtain the following truncated evolution equations:

$$J^{(0,0)}_k = A_k = \pi a_k b_k = \text{const}, \tag{3.8}$$

$$\dot{x}_k = \left[1 + \frac{1}{2A_k}(J^{(2,0)}_k \partial_x^2 + 2J^{(1,1)}_k \partial_x\partial_y + J^{(0,2)}_k \partial_y^2)\right]\begin{pmatrix}\partial_y \\ -\partial_x\end{pmatrix}\Psi_k(x)|_{x=x_k}. \tag{3.9}$$

$$\mathring{J}^{(2,0)}_k = \mathring{J}^{(2,0)}_{*k} + \{2J^{(2,0)}_k \partial_x\partial_y + 2J^{(1,1)}_k \partial_y^2\}\Psi_k(x)|_{x=x_k}, \tag{3.10}$$

$$\mathring{J}^{(0,2)}_k = \mathring{J}^{(0,2)}_{*k} + \{-2J^{(0,2)}_k \partial_x\partial_y + 2J^{(1,1)}_k \partial_y^2\}\Psi_k(x)|_{x=x_k}, \tag{3.11}$$

$$\mathring{J}^{(1,1)}_k = \mathring{J}^{(1,1)}_{*k} + (J^{(2,0)}_k + J^{(0,2)}_k)\partial_y^2 \Psi_k(x)|_{x=x_k}. \tag{3.12}$$

Here we use the truncated far-field expansion stream function

$$\Psi_k(x) = -\sum_{\alpha=1}^{N}{}' \frac{\omega_\alpha A_\alpha}{2\pi}\left\{\ln R_\alpha + \frac{A_\alpha}{8\pi R_\alpha^2}\frac{1-\lambda_\alpha^2}{\lambda_\alpha}\cos 2(\theta_\alpha - \phi_\alpha)\right\}, \tag{3.13}$$

where R_α and θ_α are defined through

$$x - x_\alpha = R_\alpha(\cos\theta_\alpha, \sin\theta_\alpha). \tag{3.14}$$

Since we have assumed all FAVORs to be ellipses, we have five unknowns, x_k, y_k, A_k, λ_k and ϕ_k, and six equations for each FAVOR. Therefore the system (3.8)–(3.12) is either overdetermined or it is possible to derive the area conservation (3.8) from the moment evolution equations (3.10)–(3.12). For an ellipse the area is related to the moments of inertia through

$$\frac{A_k^4}{16\pi^2} = J^{(2,0)}_k J^{(0,2)}_k - J^{(1,1)}_k J^{(1,1)}_k. \tag{3.15}$$

We calculate the time derivative of this expression using the moment evolution equations (3.10)–(3.12), and find that the time derivative of the right-hand side of (3.15) vanishes. Therefore area conservation is implied by the moment evolution equations. If we define the axis of the ellipse by

$$a_k = \left(\frac{\lambda_k A_k}{\pi}\right)^{\frac{1}{2}}, \quad b_k = \left(\frac{A_k}{\pi\lambda_k}\right)^{\frac{1}{2}}, \quad A_k = \pi a_k(0)\, b_k(0), \tag{3.16}$$

we maintain the area conservation, and one of the moment evolution equations can be omitted. Thus we now only have the variables λ_k, ϕ_k, $\boldsymbol{x}_k$ and the constants A_k, ω_k.

We shall now derive equations governing $\dot{\lambda}_k$ and $\dot{\phi}_k$. The sum and difference of the main moments are

$$S_k \equiv J_k^{(2,0)} + J_k^{(0,2)} = \frac{A_k^2}{4\pi}\frac{1+\lambda_k^2}{\lambda_k}, \tag{3.17}$$

$$D_k \equiv J_k^{(2,0)} - J_k^{(0,2)} = -\frac{A_k^2}{4\pi}\frac{1-\lambda_k^2}{\lambda_k}\cos 2\phi_k. \tag{3.18}$$

We differentiate (3.17) and (3.18), apply the moment evolution equations and obtain

$$\dot{\lambda}_k = \lambda_k \sum_{\alpha=1}^{N}{}' \frac{\omega_\alpha}{\pi}\frac{A_\alpha}{R_{k\alpha}^2}\sin 2(\theta_{k\alpha} - \phi_k), \tag{3.19}$$

and

$$\dot{\phi}_k = \omega_k \frac{\lambda_k}{(1+\lambda_k)^2} + \frac{1+\lambda_k^2}{1-\lambda_k^2}\sum_{\alpha=1}^{N}{}' \frac{\omega_\alpha A_\alpha}{2\pi}\frac{\cos[2(\theta_{k\alpha}-\phi_k)]}{R_{k\alpha}^2}, \tag{3,20}$$

where $\boldsymbol{x}_k - \boldsymbol{x}_\alpha \equiv R_{k\alpha}(\cos\theta_{k\alpha}, \sin\theta_{k\alpha})$. Obviously, (3.20) has a singularity for $\lambda_k = 1$ owing to the fact that ϕ_k is not defined for $\lambda_k = 1$. Equations (3.19) and (3.20) are multi-FAVOR generalizations of Kida's equation (2.9) for one elliptical vortex in a strain field. In order to obtain a suitable set of equations for numerical studies, we remove the singularity by introducing

$$(\delta_k, \gamma_k) = \left(\frac{A_k}{8\pi\lambda_k}\right)^{\frac{1}{2}}(\lambda_k - 1)(\cos 2\phi_k, \sin 2\phi_k). \tag{3.21}$$

Equations (3.19) and (3.20) become

$$\dot{\delta}_k = \frac{-\omega_k \gamma_k}{2 + \frac{4\pi}{A_k}(\delta_k^2 + \gamma_k^2)} + \sum_{\alpha=1}^{N}{}' \frac{\Gamma_\alpha\left[\gamma_k\delta_k\cos 2\theta_{k\alpha} + \left(\delta_k^2 + 2\gamma_k^2 + \frac{A_k}{2\pi}\right)\sin 2\theta_{k\alpha}\right]}{2\pi R_{k\alpha}^2\left(\delta_k^2 + \gamma_k^2 + \frac{A_k}{2\pi}\right)^{\frac{1}{2}}} \tag{3.22}$$

and

$$\dot{\gamma}_k = \frac{\omega_k \delta_k}{2 + \frac{4\pi}{A_k}(\delta_k^2 + \gamma_k^2)} - \sum_{\alpha=1}^{N}{}' \frac{\Gamma_\alpha\left[\gamma_k\delta_k\sin 2\theta_{k\alpha} + \left(2\delta_k^2 + \gamma_k^2 + \frac{A_k}{2\pi}\right)\cos 2\theta_{k\alpha}\right]}{2\pi R_{k\alpha}^2\left(\delta_k^2 + \gamma_k^2 + \frac{A_k}{2\pi}\right)^{\frac{1}{2}}}, \tag{3.23}$$

where $\Gamma_\alpha = A_\alpha\omega_\alpha$. These equations do not have any singularities as long as H1 is satisfied. (However, if H1 is not fulfilled $R_{k\alpha}$ may be small and we are in serious trouble numerically.)

The equation for the centroid motion is

$$\begin{pmatrix}\dot{x}_k\\ \dot{y}_k\end{pmatrix} = \sum_{\alpha=1}^{N}{}' \frac{\omega_\alpha A_\alpha}{2\pi R_{k\alpha}}\left\{\begin{matrix}-\sin\theta_{k\alpha}\\ \cos\theta_{k\alpha}\end{matrix} + \frac{A_\alpha}{4\pi R_{k\alpha}^2}\frac{1-\lambda_\alpha^2}{\lambda_\alpha}\begin{pmatrix}\sin(3\theta_{k\alpha}-2\phi_\alpha)\\ -\cos(3\theta_{k\alpha}-2\phi_\alpha)\end{pmatrix}\right.$$
$$\left. + \frac{A_k}{4\pi R_{k\alpha}^2}\frac{1-\lambda_k^2}{\lambda_k}\begin{pmatrix}\sin(3\theta_{k\alpha}-2\phi_k)\\ -\cos(3\theta_{k\alpha}-2\phi_k)\end{pmatrix}\right\} \quad (3.24)$$

or, in terms of the variables (γ_k, δ_k),

$$\begin{pmatrix}\dot{x}_k\\ \dot{y}_k\end{pmatrix} = \sum_{\alpha=1}^{N}{}' \frac{\omega_\alpha A_\alpha}{2\pi R_{k\alpha}}\left\{\begin{matrix}-\sin\theta_{k\alpha}\\ \cos\theta_{k\alpha}\end{matrix} - \frac{2}{R_{k\alpha}^2}\left(\delta_k^2+\gamma_k^2+\frac{A_k}{2\pi}\right)^{\frac{1}{2}}\begin{pmatrix}\delta_k\sin 3\theta_{k\alpha}-\gamma_k\cos 3\theta_{k\alpha}\\ -\delta_k\cos 3\theta_{k\alpha}-\gamma_k\sin 3\theta_{k\alpha}\end{pmatrix}\right.$$
$$\left. - \frac{2}{R_{k\alpha}^2}\left(\delta_\alpha^2+\gamma_\alpha^2+\frac{A_\alpha}{2\pi}\right)^{\frac{1}{2}}\begin{pmatrix}\delta_\alpha\sin 3\theta_{k\alpha}-\gamma_\alpha\cos 3\theta_{k\alpha}\\ -\delta_\alpha\cos 3\theta_{k\alpha}-\gamma_\alpha\sin 3\theta_{k\alpha}\end{pmatrix}\right\}. \quad (3.25)$$

Thus the equations constituting our numerical model are (3.22), (3.23) and (3.25).

The moment model is complete in every order, and the explicit shape of a FAVOR is not a consideration in the derivation of the evolution equations.

4. Conserved quantities

The 2-dimensional Euler equations conserve the following:
functional of vorticity $F(\omega)$

$$\frac{\mathrm{d}}{\mathrm{d}t}\int_{\mathbb{R}^2} F(\omega)\,\mathrm{d}\sigma = 0; \quad (4.1)$$

global centroid

$$\frac{\mathrm{d}}{\mathrm{d}t}\int_{\mathbb{R}^2} \boldsymbol{x}\omega\,\mathrm{d}\sigma = 0; \quad (4.2)$$

angular impulse

$$\frac{\mathrm{d}}{\mathrm{d}t}\int_{\mathbb{R}^2} \boldsymbol{x}\cdot\boldsymbol{x}\omega\,\mathrm{d}\sigma = 0; \quad (4.3)$$

excess energy (see Batchelor 1967, §7.3)

$$-\tfrac{1}{2}(\mathrm{d}/\mathrm{d}t)\int_{\mathbb{R}^2}\omega\psi\,\mathrm{d}\sigma = 0. \quad (4.4)$$

For contour dynamics and the moment models, the first three are conserved. In both cases, (4.1) corresponds to area conservation. In both cases, the centroid is conserved because the velocity field is a double integral over a kernel with odd symmetry. Finally, in both cases the rate of change of angular impulse is

$$\dot{M} = 2\int_{\mathbb{R}^2}(xu+yv)\,\omega\,\mathrm{d}\sigma,$$

which vanishes because $\boldsymbol{u} = \nabla\times\boldsymbol{e}_z\psi$ and ψ is an integral over a kernel which depends

only on a scalar distance. For reference, we write M for the second-order moment model:

$$\begin{aligned} M &\equiv \int_{\mathbb{R}^2} \omega \boldsymbol{x}\cdot\boldsymbol{x}\,\mathrm{d}\sigma \\ &= \sum_{k=1}^{N} \omega_k \int_{D_k} [(x_k+\xi_k)^2+(y_k+\eta_k)^2]\,\mathrm{d}\sigma \\ &= \sum_{k=1}^{N} \omega_k A_k(x_k^2+y_k^2)+\omega_k(J_k^{(2,0)}+J_k^{(0,2)}) \\ &= \sum_{k=1}^{N} \Gamma_k\left[\boldsymbol{x}_k\cdot\boldsymbol{x}_k+\frac{A_k}{4\pi}\frac{1+\lambda_k^2}{\lambda_k}\right]. \end{aligned} \tag{4.5}$$

Here the first term is the same as in the point-vortex model while the second is a correction due to the ellipticity of the FAVOR.

For the second-order model we calculate the excess energy as

$$H \equiv -\frac{1}{2}\int_{\mathbb{R}^2} \omega\psi\,\mathrm{d}\sigma = -\sum_{k=1}^{N} \tfrac{1}{2}\omega_k \int_{D_k} (\psi_k+\Psi_k)\,\mathrm{d}\sigma, \tag{4.6}$$

where the first term is the self-energy of the kth FAVOR while the second term is the interaction energy. We prefer to use a stream function ψ whose asymptotic representation does not contain a constant term. This requires introducing a normalization length

$$L = \ln \prod_{k=1}^{N} (\Gamma_k/\pi\omega_k)^{\Gamma_k/2\Gamma}, \quad \Gamma \equiv \sum_{k=1}^{N} |\Gamma_k|,$$

since

$$\begin{aligned} \psi = \sum_{k=1}^{N} \psi_k &= -\frac{1}{4\pi}\sum_{k=1}^{N}\int_{D_k} \omega(\xi,\eta)\ln\left[\frac{(x-\xi)^2+(y-\eta)^2}{\Gamma_k/\omega_k\pi}\right]\mathrm{d}\sigma \\ &= -\frac{1}{4\pi}\left\{\int_{\mathbb{R}^2} \omega(\xi,\eta)\ln[(x-\xi)^2+(y-\eta)^2]\,\mathrm{d}\sigma - \Gamma\sum_{k=1}^{N}\frac{\Gamma_k}{\Gamma}\ln\left(\frac{\Gamma_k}{\omega_k\pi}\right)\right\} \\ &= -\frac{1}{2\pi}\sum_{k=1}^{N}\Gamma_k \ln\left(\frac{r}{(\Gamma_k/\omega_k\pi)^{\frac{1}{2}}}\right)+O\left(\frac{1}{r}\right). \end{aligned}$$

Thus for an elliptical FAVOR with major axis parallel to the x-axis the inner stream function, by continuity with the outer, becomes

$$\psi = -\frac{\omega(x^2+\lambda y^2)}{2(\lambda+1)} - \frac{\Gamma}{4\pi}\ln\left(\frac{(1+\lambda)^2}{4\lambda}\right)+\frac{\Gamma}{4\pi}, \tag{4.7}$$

subject to the length unit $(A/\pi)^{\frac{1}{2}}$. Since the normalization constant depends on λ, it is of importance for the calculation of H by (4.4). The expression for the self-energy becomes

$$H_{*k} = -\int_{D_k} \tfrac{1}{2}\omega_k\psi_k\,\mathrm{d}\sigma = +\frac{\Gamma_k^2}{8\pi}\ln\left(\frac{(1+\lambda_k)^2}{4\lambda_k}\right)-\frac{\Gamma_k^2}{16\pi}, \tag{4.8}$$

which has a minimum at $\lambda_k = 1$. The interaction energy is given through

$$
\begin{aligned}
-\tfrac{1}{2}\omega_k \int_{D_k} \Psi_\kappa \,\mathrm{d}\sigma &= +\omega_k \sum_{\alpha=1}^{N}{}' \frac{\omega_\alpha}{4\pi} \int_{D_k} \Psi_{k\alpha}\,\mathrm{d}\sigma \\
&= +\sum_{\alpha=1}^{N}{}' \frac{\omega_k \omega_\alpha}{4\pi} \int_{D_k} \Big\{1 + \xi\frac{\partial}{\partial\xi} + \eta\frac{\partial}{\partial\eta} \\
&\quad + \frac{\xi^2}{2}\partial_\xi^2 + \xi\eta\,\partial_\xi\partial_\eta + \frac{\eta^2}{2}\partial_\eta^2 + \ldots\Big\} \Psi_{k\alpha}|_{x_k}\,\mathrm{d}\sigma \\
&= +\sum_{\alpha=1}^{N}{}' \frac{\omega_k \omega_\alpha}{4\pi} \{A_k + \tfrac{1}{2}J_k^{(2,0)}\partial_\xi^2 + J_k^{(1,1)}\partial_\xi\partial_\eta + \tfrac{1}{2}J_k^{(0,2)}\partial_\eta^2 + \ldots\}\, \Psi_{k\alpha}|_{x_k}.
\end{aligned}
\tag{4.9}
$$

Now we apply the same approximation to $\Psi_{k\alpha}$ as in Section 3, that is, $\Psi_{k\alpha}$ is a polynomial of second degree. Thus the infinite series above truncates after the second-order moments, and we obtain

$$
\begin{aligned}
-\tfrac{1}{2}\omega_k \int_{D_k} \Psi_k \mathrm{d}\sigma &= +\sum_{\alpha=1}^{N} \frac{\omega_k \omega_\alpha}{4\pi} \left\{A_k\, \Psi_{k\alpha}(x_k) + \frac{A_\alpha A_k (1-\lambda_k^2)}{8\pi\lambda_k R_{k\alpha}^2} \cos\left(2(\phi_k - \theta_{k\alpha})\right)\right\} \\
&= +\sum_{\alpha=1}^{N} \frac{\Gamma_k \Gamma_\alpha}{4\pi} \left\{\ln R_{k\alpha} + \frac{1}{8\pi R_{k\alpha}^2}\left[A_\alpha \frac{(1-\lambda_\alpha^2)}{\lambda_\alpha} \cos\left(2(\theta_{k\alpha} - \phi_\alpha)\right)\right.\right. \\
&\quad \left.\left. + A_k \frac{1-\lambda_k^2}{\lambda_k} \cos\left(2(\theta_{k\alpha} - \phi_k)\right)\right]\right\}.
\end{aligned}
\tag{4.10}
$$

Combining (4.8) and (4.10), we find

$$
\tilde{H} = H_* + H_C + H_I, \tag{4.11}
$$

where

$$
\left.
\begin{aligned}
H_* &= +\sum_{k=1}^{N} \frac{\Gamma_k^2}{8\pi} \ln\left(\frac{(1+\lambda_k)^2}{4\lambda_k}\right) - \frac{\Gamma_k^2}{16\pi}, \\
H_C &= +\sum_{k=1}^{N} \sum_{\alpha=1}^{N}{}' \frac{\Gamma_\alpha \Gamma_k}{4\pi} \ln R_{k\alpha}, \\
H_I &= +\sum_{k=1}^{N} \sum_{\alpha=1}^{N}{}' \frac{\Gamma_\alpha \Gamma_k}{32\pi^2 R_{k\alpha}^2}\left[A_\alpha \frac{1-\lambda_\alpha^2}{\lambda_\alpha} \cos\left(2(\theta_{k\alpha} - \phi_\alpha)\right) + A_k \frac{1-\lambda_k^2}{\lambda_k} \cos\left(2(\theta_{k\alpha} - \phi_k)\right)\right].
\end{aligned}
\right\}
\tag{4.12}
$$

The tilde ˜ indicates a truncated expansion of H in (4.6), H_* is the self- (or internal) energy and is evaluated exactly for elliptical FAVORs, H_C, depends only on the intercentroid distances (and is identical with the energy of N point vortices), and H_I is an interaction energy correct to the leading term in the small parameter (the second-order model).

The time derivative of $\tilde{H}$ is

$$
\frac{\mathrm{d}\tilde{H}}{\mathrm{d}t} = \sum_{k=1}^{N} [\dot{x}_k \partial_{x_k}\tilde{H} + \dot{y}_k \partial_{y_k}\tilde{H} + \dot{\lambda}_k \partial_{\lambda_k}\tilde{H} + \dot{\phi}_k \partial_{\phi_k}\tilde{H}]. \tag{4.13}
$$

By inspection we find

$$
\Gamma_k \dot{y}_k = \partial_{x_k}\tilde{H}, \tag{4.14}
$$

$$
\Gamma_k \dot{x}_k = -\partial_{y_k}\tilde{H} \tag{4.15}
$$

(similar to the Hamiltonian form of the point-vortex model). For the other variables we find

$$\frac{\Gamma_k A_k}{8\pi}\frac{1-\lambda_k^2}{\lambda_k^2}\dot{\phi}_k = -\partial_{\lambda_k}\tilde{H}, \tag{4.16}$$

$$\frac{\Gamma_k A_k}{8\pi}\frac{1-\lambda_k^2}{\lambda_k^2}\dot{\lambda}_k = \partial_{\phi_k}\tilde{H}. \tag{4.17}$$

Substituting (4.14)–(4.17) into (4.13) yields the energy conservation for the second-order moment model. A set of canonical variables for (4.16) and (4.17) is

$$\left(\frac{\Gamma_k A_k}{16\pi}\frac{(\lambda_k-1)^2}{\lambda_k}, 2\phi_k\right),$$

as seen by inspection. Another set, useful in numerical simulations, is (δ_k, γ_k), defined in (3.21). In these variables the Hamiltonian is

$$\begin{aligned}\tilde{H} = \frac{1}{8\pi}\sum_{k=1}^{N}\Bigg\{\Gamma_k^2 \ln\left(1+\frac{2\pi}{A_k}(\delta_k^2+\gamma_k^2)\right) - \frac{\Gamma_k^2}{2} + \sum_{\alpha=1}^{N}{}' \Gamma_k\Gamma_\alpha \ln R_{k\alpha}^2 \\ - \sum_{\alpha=1}^{N}{}' \frac{2\Gamma_k\Gamma_\alpha}{R_{k\alpha}^2}\Bigg[\left(\delta_\alpha^2+\gamma_\alpha^2+\frac{A_\alpha}{2\pi}\right)^{\frac{1}{2}}(\delta_\alpha\cos 2\theta_{k\alpha}+\gamma_\alpha\sin 2\theta_{k\alpha}) \\ +\left(\delta_k^2+\gamma_k^2+\frac{A_k}{2\pi}\right)^{\frac{1}{2}}(\delta_k\cos 2\theta_{k\alpha}+\gamma_k\sin 2\theta_{k\alpha})\Bigg]\Bigg\}.\end{aligned} \tag{4.18}$$

Furthermore, the evolution equations satisfy

$$\Gamma_k\dot{\gamma}_k = \frac{\partial H}{\partial\delta_k} \tag{4.19}$$

and

$$\Gamma_k\dot{\delta}_k = -\frac{\partial H}{\partial\gamma_k}. \tag{4.20}$$

Note the invariance of $\tilde{H}$ (H in the elliptical order) follows because the internal stream function (4.7) is a quadratic polynomial which is consistent with the quadratic polynomials that describe the far-field stream function (2.16) in this order.

5. Computational examples

In this section we apply the second-order moment model to a few well-known problems. We demonstrate its validity by showing that it is capable of accurately describing solutions of the Euler equations that have been found by the CD-method.

5.1. *Steady-state solutions – 'EV-states'*

The model is particularly simple when applied to steady-state solutions. First we will compare doubly-connected symmetric corotating states. A parameter table for V-state solutions of Euler equations can be found in Overman & Zabusky (1982).

The model steady-state solutions or 'EV-states' are obtained from (3.19), (3.20) and (3.24) with symmetric ellipses of area A at (x_1, y_1) and $(-x_1, -y_1)$ and vorticity density $\omega_1 = \omega_2 = \omega$. These states are characterized by the dimensionless centroid separation $\mu = R_{12}(\pi/A)^{\frac{1}{2}}$. For steady-state solutions we set $\dot{\lambda} = 0$ and obtain from (3.19) $\theta = \phi \bmod \frac{1}{2}\pi$. Substituting this into (3.20), we find that $\dot{\phi} = \dot{\theta}$ is constant in time. From (3.24) we obtain $\mathrm{d}R_{12}^2/\mathrm{d}t = 0$ and

$$\dot{\theta} = \frac{\omega}{\mu^2}\left[1-\frac{1}{2\mu^2}\frac{1-\lambda^2}{\lambda}\right].$$

Since $\dot{\phi} = \theta$, we obtain from (3.20) an equation for the aspect ratio λ:

$$\frac{1}{\mu^2}\left[1-\frac{1}{2\mu^2}\frac{1-\lambda^2}{\lambda}\right] = \frac{\lambda}{(1+\lambda)^2}+\frac{1+\lambda^2}{1-\lambda^2}\frac{1}{2\mu^2}, \tag{5.1}$$

which is equivalent to the quintic equation

$$0 = \lambda^5+(1+3\mu^2)\lambda^4+(3\mu^2-2\mu^4-2)\lambda^3-(2+\mu^2-2\mu^4)\lambda^2+(1-\mu^2)\lambda+1. \tag{5.2}$$

We find physically meaningful roots for $\mu \geqslant \mu_{R^*} \approx 2.9384$. There are two: one that approaches 1 as μ tends to infinity. In the limit $\mu \to \mu_{R^*}\downarrow$ these two roots form a double root $\lambda_{R^*} \approx 2.05$, as shown in the (μ^{-1}, λ^{-1})-diagram of figure 2.

The stability of these corotating EV-states can be determined theoretically. We express the parameter μ in terms of λ and the moment of inertia M (which is a conserved quantity of the model):

$$2\mu^2 = \frac{4\pi M}{\Gamma A}-\frac{2(\lambda^2+1)}{\lambda}. \tag{5.3}$$

Hence we write (3.19)–(3.21) in the abstract form

$$\frac{\mathrm{d}\boldsymbol{Y}}{\mathrm{d}t} = \boldsymbol{F}(\boldsymbol{Y};\sigma), \tag{5.4}$$

where $\boldsymbol{Y} = (x, y, \lambda, \phi)$ and $\sigma = 4\pi M/\Gamma A$ is a constant of motion. According to the factorization theorem of Joseph & Nield (1975) there is an exchange of stability of the steady states at the *minimum* value of σ, because this is a turning point in the (σ, λ)-diagram. Numerically, the turning point is obtained for $\mu = \mu_{\mathrm{cr}} \approx 2.9396$ ($\lambda_{\mathrm{cr}} \approx 2.36$). Clearly, the solid solution branch of figure 2 is the stable one since $\lambda \to 1$ as $\mu \to \infty$; hence the other branch is unstable. This result compares favourably with the estimate of Saffman & Szeto (1980) and Dritschel (1985). They used the symmetric corotating contour-dynamical V-states and predicted instability for $\mu < 3.16$ and $\mu < 3.20$ respectively.

Table 1 compares results obtained from the present model, a point-vortex equivalent and the 'exact' CD-solutions. From this table we see good agreement between the Euler equations and our model even in cases where the perturbation parameter is large. Note that the aspect ratio for the CD-results is not based on second-order moments but is simply the length of a FAVOR divided by the width. Because the states corresponding to large values of the perturbation parameter are more almond-shaped (see Overman & Zabusky 1982) than the ellipse, the model may give an aspect ratio that is actually better than appears from the table. Furthermore, we notice that the model yields a much better approximation to the angular velocity than the point-vortex model.

Next, we consider the doubly connected, symmetric, translating EV-states of our model. Let two elliptical FAVORs with the same area A and aspect ratio λ, but opposite-signed vorticity densities be situated symmetrically around the x-axis as shown in figure 3.

The steady-state requirement $\dot{\lambda} = 0$ implies $\theta = \phi \bmod \frac{1}{2}\pi$, and thereby $\dot{\phi} = \theta = 0$. Thus the state propagates in the x-direction with velocity

$$\dot{x} = \frac{\omega A}{2\pi R_{12}}\left[1-\frac{A}{2\pi R_{12}^2}\frac{\lambda^2-1}{\lambda}\right], \tag{5.5}$$

or

$$\dot{x} = \omega\left[1-\frac{\lambda^2-1}{2\lambda\mu^2}\right]\Big/\left[\mu^2+\frac{2\mu}{\lambda^{\frac{1}{2}}}\right], \tag{5.6}$$

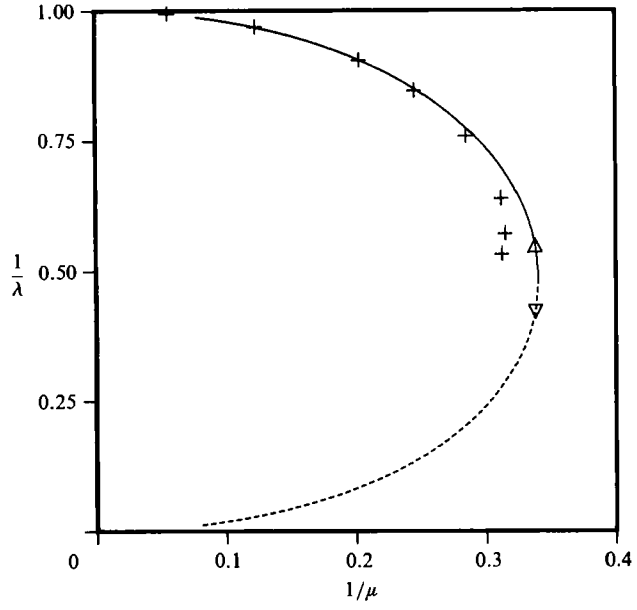

FIGURE 2. Reciprocal aspect ratio λ^{-1} versus reciprocal dimensionless centroid separation μ^{-1} for symmetric corotating EV-states. The solid line and dashed line represent linearly stable and unstable regimes respectively. The (+) show comparable CD results given in Overman & Zabusky (1982). The (∇) ($\mu = 2.960$, $\lambda = 2.374$) corresponds to the unstable evolution shown in figures 5(*a*, *b*), and (Δ) ($\mu = 2.960$, $\lambda = 1.819$) corresponds to the stable evolution shown in figure 5(*c*).

		Contour dynamics		Moment model		Point vortex
No.†	μ	$\frac{1}{\lambda}$	$\frac{d\theta}{dt}$	$\frac{1}{\lambda}$	$\frac{d\theta}{dt}$	$\frac{d\theta}{dt}$
1	18.0542	0.9943	0.003068	0.9938	0.003068	0.003068
3	8.1322	0.9685	0.01513	0.9683	0.01513	0.01512
5	4.9210	0.9044	0.04146	0.9052	0.04146	0.04129
6	4.0684	0.8499	0.06108	0.8499	0.06101	0.06042
7	3.5054	0.7597	0.08344	0.7747	0.08309	0.08138
8	3.2052	0.6395	0.1027	0.6983	0.1008	0.09733
9	3.1742	0.5726	0.1073	0.6871	0.1030	0.09925
10	3.2004	0.5342	0.1074	0.2787	0.1134	0.09763

† The number in the first column refers to the contour number in figure 1 of Overman & Zabusky (1982).

TABLE 1. Comparison between contour dynamics and the moment model for symmetric doubly connected rotating V-states

where $\mu = R_{12}(\pi/A)^{\frac{1}{2}}$ and we have normalized lengths such that

$$2 \equiv 2b + R_{12} = 2\left(\frac{A}{\pi\lambda}\right)^{\frac{1}{2}} + R_{12},$$

so that

$$R_{12} = 2\Big/\left[1 + \frac{2}{\mu\lambda^{\frac{1}{2}}}\right]. \tag{5.7}$$

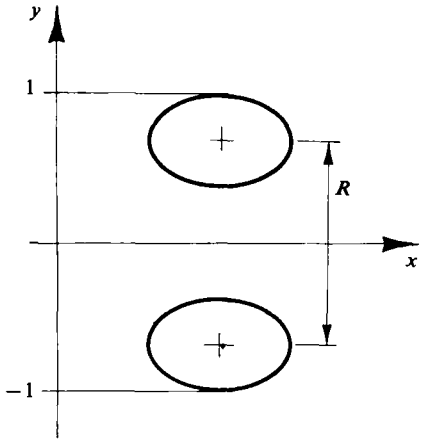

FIGURE 3. Schematic of a translating EV-state.

Using (3.20), we find that the aspect ratio satisfies

$$0 = \frac{\lambda}{(1+\lambda)^2} + \frac{1+\lambda^2}{1-\lambda^2}\frac{1}{2\mu^2}, \tag{5.8}$$

which is equivalent to the cubic equation

$$0 = \lambda^3 + (1-2\mu^2)\,\lambda^2 + (1+2\mu^2)\,\lambda + 1. \tag{5.9}$$

For $\mu_{T^*} \approx 1.8249$ there is a double root $\lambda_{T^*} \approx 2.89$, and an unphysical negative root. For $\mu > \mu_{T^*}$ there are two positive roots, as shown in figure 4. Table 2 compares model, point-vortex and CD (Wu, Overman & Zabusky 1984) results. (For the point-vortex results the opposite circulations are separated by R_{12} given in (5.7).) For translating EV-states we cannot use the factorization theorem because $\Gamma = 0$ and no appropriate constant of the motion is available. Instead, the stability of the states is determined by a numerical study. As shown in figure 4, the exchange of stability occurs at $\mu = \mu_{T_{\rm cr}} \approx 1.8269$, $\lambda_{T_{\rm cr}} \approx 2.73$, where the solid curve is the stable region and the dashed curve the unstable region.

5.2. *Dynamical simulations*

We investigate the stability and long-time evolution of the perturbed stationary corotating EV-states located at the triangles on figure 2 via numerical solutions of (3.22), (3.23) and (3.25). The perturbations are selected to keep A, Γ and $\sigma(=4\pi M/\Gamma A)$ the same as for the unperturbed state. The simplest perturbation satisfying this restriction is obtained by changing the orientation of the ellipses. (Note that (4.5) shows that M is independent of ϕ.)

The state (V) is linearly unstable to a symmetric perturbation $\phi_1(0) = \phi_2(0) = \delta$. However, the long-time evolution is sensitive to the sign of δ. If δ is negative, $\delta = -0.001°$, the centroid distance decreases monotonically, and vanishes at $t = 0.761$, a process we call '*collapse*'. (Obviously, the assumptions on which the model are based have been violated during this time.) Figure 5(*a*) shows the initial divergent evolution of $\log_{10}(R_{12}(t)/R_{12}(0))$ (solid curve) and $\log_{10}(\lambda(t)/\lambda(0))$ (dashed curve). For $\delta = 0.001°$ we get an initial exponential divergence and long-time recurrence, with $t_R = 1.15$ as shown in figure 5(*b*). Note that the intercentroid distance does not decrease below its initial value, and periodically increases to $R_{12}/R_{12}(0) = 1.04$.

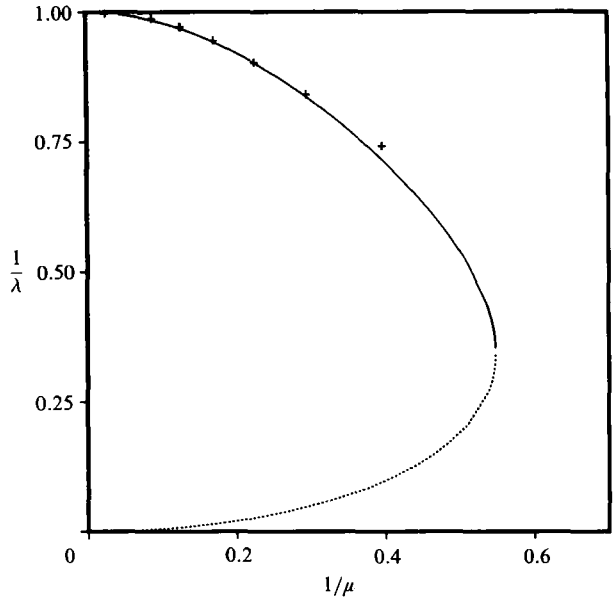

FIGURE 4. Same coordinates as figure 2 for a symmetric translating EV-state. The solid and dashed lines correspond to linearly stable and unstable regimes, respectively. The (+) show comparable CD-results from Wu *et al.* (1984).

		Contour dynamics		Moment model		Point vortex
No.†	μ	λ	$\frac{dx}{dt}$	λ	$\frac{dx}{dt}$	$\frac{dx}{dt}$
1	37.98	1.001	6.64′–4	1.001	6.57′–4	6.57′–4
2	17.94	1.006	2.79′–3	1.006	2.78′–3	2.78′–3
3	11.25	1.016	6.72′–3	1.016	6.69′–3	6.69′–3
4	7.865	1.033	0.0129	1.033	0.0129	0.0129
5	5.822	1.061	0.0221	1.061	0.0221	0.0221
6	4.416	1.107	0.0355	1.108	0.0355	0.0357
7	3.375	1.188	0.0557	1.195	0.0558	0.0567
8	2.518	1.348	0.0885	1.399	0.0890	0.0941
9	1.721	1.747	0.149		no solution	

† The number in the first column refers to the contour number in table 1 of Wu *et al.* (1984).

TABLE 2. Comparison between contour dynamics and the moment model for symmetric doubly connected translating V-states

Similarly the aspect ratio decreases periodically to $\lambda(t)/\lambda(0) = 0.549$, a more circular state.

The state (Δ) is linearly stable, and figure 5(*c*) shows the results of imposing an unsymmetrical perturbation $\delta = 1°$, much larger than imposed on the unstable states. For the time shown, the response remains small and the intercentroid distance is quasi-periodic.

For the translating EV-states, we imposed several types of perturbations and conclude that there are two types of instabilities for $\lambda > 2.73$. We illustrate the first type in figure 6(*a*), where the 2.89:1 ellipses are perturbed symmetrically with

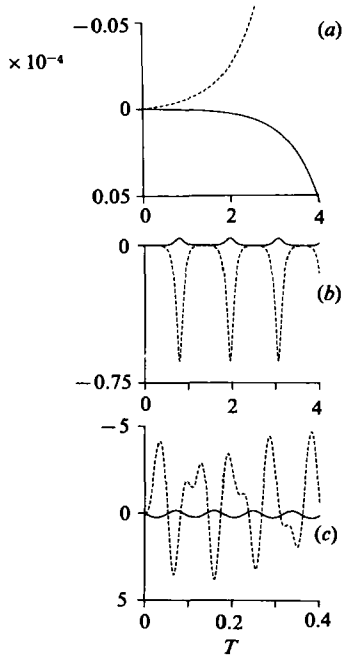

FIGURE 5. Diagnostics $\ln|R_1(t)/R_1(0)|$ (——) and $\ln|\lambda_1(t)/\lambda_1(0)|$ (– – – –) for the evolution of perturbed unstable and stable corotating EV-states at $\mu = 2.960$: (*a*) unstable, $\lambda^{-1}(0) = 0.42123$, $\phi_1(0) = \phi_2(0) = -0.001°$; (*b*) unstable, $\lambda_1^{-1}(0) = 0.42123$, $\phi_1(0) = \phi_2(0) = +0.001°$; (*c*) stable, $\lambda_1^{-1}(0) = 0.54970$, $\phi_1(0) = -1.0°$, $\phi_2(0) = 0$. (In all cases $\omega_1 = \omega_2 = 100.0$.)

$(\phi_U, \phi_L) = (-1°, +1°)$. (Note U ≡ upper and L ≡ lower.) We observe a monotonic increase of aspect ratio and $|\phi|$ and a decrease of centroid velocity. After $t = 24$, where $\lambda = 4.3$, the aspect ratio increases rapidly and the model becomes invalid. One observes the bizarre unphysical result that the elongating state reverses its propagation direction. Note that during this calculation the intercentroid separation is time-independent, as can be verified from the equations of motion.

The evolution of the second asymmetric instability is shown in figure 6(*b*). Here the 2.89:1 ellipses are perturbed with $(\phi_U, \phi_L) = (-1°, 0°)$, and we observe that the upper ellipse elongates monotonically while the lower remains undisturbed. This causes a dramatic change in propagation direction, an indication that the upper FAVOR would be wrapped around the lower in a CD-simulation. Such a response would probably cause the FAVOR pair to enter a curved orbit.

We now validate the model by comparing with a non-merging CD-solution. We begin with two circular FAVORs, the left with radius $R_1 = 1.0$, and the right with radius $R_2 = 0.2$, and an intercentroid distance $R_{12} = 2.0$. The small FAVOR has vorticity density 2.5 while the large has $\omega = 1$. (Note that the parameters for this run were incorrectly given in the text and figure caption of Melander *et al.* (1984).) This stable situation was calculated by Overman & Zabusky (1982). Our results are shown in figure 7 and comparisons are made in table 3. (Note that for the CD-solutions λ and ϕ are obtained by fitting second-order moments to the contours.) For the model the solution is quasi-periodic with periods $\bar{T}_1 = 63.2$ and $\bar{T}_2 = 14.5$ for the aspect ratio of the larger and smaller FAVOR respectively. For the CD-solutions the comparable periods are $T_1 = 66.7$ and $T_2 = 15.3$, a good result considering that the perturbation parameter $\mu^{-1} \approx (A_1/\pi)^{\frac{1}{2}}/R_{12} \approx 0.5$, is not small. The CD-solution is known only for

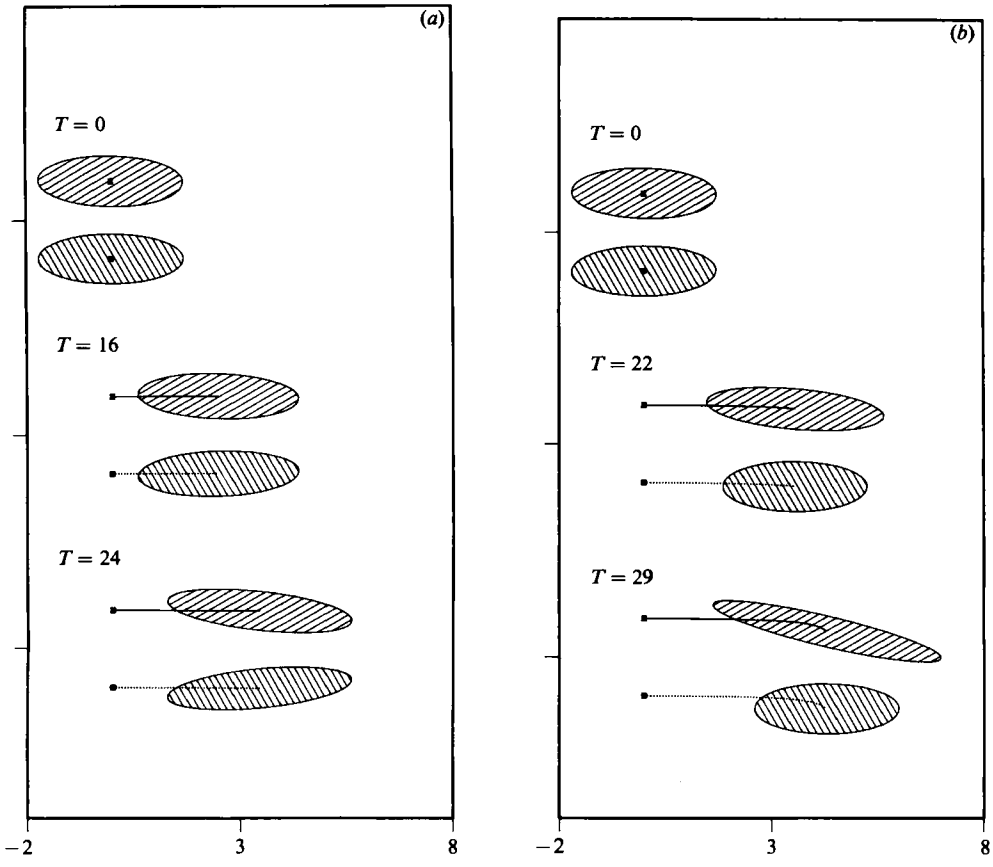

FIGURE 6. Evolution of translating EV-states of aspect ratio 2.89 and $\omega_U = -\omega_L = 1.0$: (*a*) symmetric perturbation $(\phi_U, \phi_L) = (-1°, +1°)$; (*b*) unsymmetric perturbation $(\phi_U, \phi_L) = (-1°, 0)$.

$t \leqslant 38$, and T_1 is obtained by extrapolation. We have continued the model solution for several hundred units of time and have continued to observe a quasi-periodic solution.

If the initial intercentroid distance is decreased from 2.0 to 1.8 the CD-simulations of Overman & Zabusky (1982) exhibit a merger at $t \approx 20.0$. For our model this change in initial conditions leads to a *collapse* of the centroids at $t_c = 25.4$, that is, where $R_{12}(t_c) = 0$. Furthermore, for two *identical* circular FAVORs at $t = 0$, CD-simulations of Zabusky, Hughes & Roberts (1979) show a merger occurring near $\mu \approx 3.40$, whereas our model shows a transition to collapse at $\mu \approx 3.2$. A third correspondence between merger and collapse occurs when one perturbs symmetric corotating V-states and corresponding EV-states. From Overman & Zabusky's CD-simulations (1982), we know that certain perturbations of unstable V-states lead to merger. For our model such perturbations result in centroid collapse.

6. Discussion and conclusions

We have introduced a general self-consistent desingularization procedure for the 2-dimensional Euler equations. Thus we have found a representation (or model) in the hierarchy *between* the point (i.e. singular) or invariant-core vortex approaches and

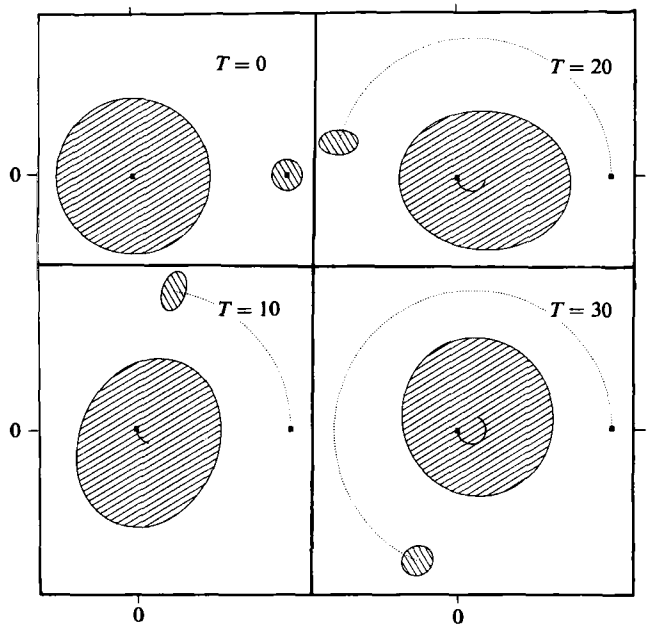

FIGURE 7. Evolution of corotating initially circular FAVORs via the moment model. A comparison with CD-results is given in table 3. Here $R_{12}(0) = 2.0$, $A_1 = \pi$, $A_2 = 0.04\pi$ and $\omega_1 = \omega_2/2.5 = 1.0$. (Note that this is the same as figure 2 in Melander *et al.* (1984), except that their figure caption is in error as well as their material in the text describing this figure.)

	R_{12}		θ_{12}		λ†		ϕ†	
t	EE	model	EE	model	EE	model	EE	model
0	2.0	2.0	0	0	1.0	1.0	—	—
10	1.966	1.969	80.8°	80.6°	1.239	1.229	245.8°	245.7°
					0.584‡	0.591	339.7°	340.3°
20	1.955	1.964	166.5°	165.1°	1.281	1.251	354.2°	355.7°
					1.812	1.593	533.7°	541.2°
30	1.995	1.998	248.8°	246.4°	1.075	1.040	464.5°	466.3°
					1.137	1.125	735.5°	748.2°
38	1.989	1.985	312.2°	310.0°	0.884‡	0.862	553.5°	555.1°
					0.964‡	0.745	942.4°	912.3°

† Upper entry is λ_1, the larger area; lower entry is λ_2, the smaller area.
‡ $\lambda < 1$ is chosen to maintain continuity of ϕ through $\lambda = 1$.

TABLE 3. Comparison of a near-periodic solution of Euler equations via contour dynamics and the model

the continuum contour-dynamical (CD) approach for FAVORs. The former involves coupled ordinary differential equations (two per vortex) and the latter coupled integrodifferential equations. Our general moment model equations of motion involve centroids and moments of many initially isolated vortex regions and are derived by an asymptotic expansion in two small parameters: d_k, related to the deviation from

circularity, and ϵ_k, proportional to the area of the FAVOR divided by the square of the interFAVOR distance. In essence, CD is easier to visualize, but more difficult to solve analytically than the moment model.

The second-order moment model given in (3.19), (3.20) and (3.24) (or (3.25)) introduces two additional dependent variables per vortex, an aspect ratio and an orientation. They are associated with an elliptical shape and are related physically to internal degrees of freedom. The model exactly conserves area (circulation), global centroid position, and angular impulse. The model forms a Hamiltonian system, with the excess energy as the Hamiltonian.

We have compared this model with contour-dynamical steady states ('V-states') and dynamical simulations and have obtained remarkably good results. In particular, the elliptically desingularized model can exhibit the 'collapse' of two vortex centres, a process mathematically analogous to the *initial* approach to merger or pairing observed for CD-simulations. For symmetric initial conditions, we can find analytical solutions (Melander *et al.* 1986). In this case the Hamiltonian system is integrable and can be reduced to a phase-plane analysis, where the trajectories are the level curves of $\tilde{H}$, (4.11). As the vortex centres approach during a merger, the model becomes increasingly invalid. It is possible that by, introducing appropriate topology changes, we will be able to continue the simulations for very long times.

In work in progress we are applying the moment method to the two-dimensional Navier–Stokes equations with very small viscosity. If we assume smooth vorticity distributions and truncate after second moments, we find that the area of each FAVOR increases while its circulation remains *constant* (and obviously the vorticity decreases), a property of the Navier–Stokes equations (Poincaré 1893). Furthermore, the global moment of inertia obeys the Poincaré identity $\partial_t M = 4\nu\Gamma$, (Poincaré 1893; Howard 1957/58), where M is given in (4.5).

This work was supported in part by the U.S. Army Research Office under Contract DAAG-29-82-K-0067. We are grateful to E. A. Overman for helpful conversations and assistance with contour-dynamical results. One of us (N.Z.) acknowledges conversations with J. Marsden and R. Montgomery as well as information from the latter which led us to find a transformation to canonical variables.

REFERENCES

AREF, H. 1983 Integrable, chaotic, and turbulent vortex motion in two-dimensional flows. *Ann. Rev. Fluid Mech.* **15**, 345–389.

BATCHELOR, G. K. 1967 *An Introduction to Fluid Mechanics.* Cambridge University Press.

BEALE, J. T. & MAJDA, A. 1984 Higher order accurate vortex methods with explicit velocity kernels. *J. Comp. Phys.* **58**, 188–208.

DRITSCHEL, D. 1985 The stability and energetics of corotating uniform vortices. *J. Fluid Mech.* **157**, 95–134.

HERNAN, M. A. & JIMENEZ, J. 1982 Computer analysis of a high-speed film of the plane turbulent mixing layer. *J. Fluid Mech.* **119**, 323–345.

HOWARD, L. N. 1957/58 *Arch. Rat. Mech. Anal.* **1**, 113–123.

JOSEPH, D. D. & NIELD, D. A. 1975 Stability of bifurcating time-periodic and steady state solutions of arbitrary amplitude. *Arch. Rat. Mech. Anal.* **58**, 369.

KIDA, S. 1981 Motion of an elliptic vortex in a uniform shear flow. *J. Phys. Soc. Japan* **50**, 3517–3520.

LEONARD, A. 1980 Vortex methods for flow simulation. *J. Comp. Phys.* **37**, 289–355.

McWILLIAMS, J. C. 1984 The emergence of isolated vortices in turbulent flow. *J. Fluid Mech.* **146**, 21–43.

MELANDER, M. V., McWILLIAMS, J. C. & ZABUSKY, N. J. 1986 A model for symmetric vortex-merger. *Trans. 3rd Army Conf. on Applied Mathematics and Computing*; *ARO Rep.* 867.

MELANDER, M. V., STYCZEK, A. S. & ZABUSKY, N. J. 1984 Elliptically desingularized vortex model for the two-dimensional Euler equations. *Phys. Rev. Lett.* **53**, 1222–1225.

NAKAMURA, Y., LEONARD, A. & SPALART, P. 1982 Vortex simulation of an inviscid shear layer. *AIAA/ASME 3rd Joint Thermophysics, Fluids, Plasma and Heat Transfer Conf.*; *Paper* AIAA-82-0948.

NEU, J. C. 1984 The dynamics of a columnar vortex in an imposed strain. *Phys. Fluids* **27**, 2397–2402.

OVERMAN, E. A. & ZABUSKY, N. J. 1982 Evolution and merger of isolated vortex structures. *Phys. Fluids* **25**, 1297–1305.

POINCARÉ, H. 1893 *Theorie des Tourbillons* (ed. G. Carre), chap. IV. Deslis Freres.

SAFFMAN, P. G. & SZETO, R. 1980 Equilibrium shapes of a pair of equal uniform vortices. *Phys. Fluids* **23**, 2339–2342.

WINANT, C. D. & BROWAND, F. K. 1974 Vortex pairing: a mechanism of turbulent mixing layer growth at moderate Reynolds number. *J. Fluid Mech.* **63**, 237–255.

WU, H. M., OVERMAN, E. A. & ZABUSKY, N. J. 1984 Steady state solutions of the Euler equations in two dimensions. Rotating and translating V-states with limiting cases. I. Numerical results. *J. Comp. Phys.* **53**, 42–71.

ZABUSKY, N. J. 1984 Contour dynamics: a method for inviscid and nearly inviscid two-dimensional flows. In *Proc. IUTAM Symp. on Turbulence and Chaotic Phenomena*, pp. 251–257. North-Holland.

ZABUSKY, N. J., HUGHES, M. H. & ROBERTS, K. V. 1979 Contour dynamics for the Euler equations in two dimensions. *J. Comp. Phys.* **30**, 96–106.